



Ageing evaluation of cable insulations subjected to radiation ageing: Application of principal component analyses to Fourier Transform Infra-Red and dielectric spectroscopy

Simone Vincenzo Suraci, Sandrine Amat, Lea Hippolyte, Astrid Maléchaux, Davide Fabiani, Claire Le Gall, Océane Juan, Nathalie Dupuy

► To cite this version:

Simone Vincenzo Suraci, Sandrine Amat, Lea Hippolyte, Astrid Maléchaux, Davide Fabiani, et al.. Ageing evaluation of cable insulations subjected to radiation ageing: Application of principal component analyses to Fourier Transform Infra-Red and dielectric spectroscopy. High Voltage, 2022, 7 (4), pp.652-665. 10.1049/hve2.12239 . hal-03739298

HAL Id: hal-03739298

<https://hal.science/hal-03739298>



Submitted on 27 Jul 2022

HAL is a multi-disciplinary open access archive for the deposit and dissemination of scientific research documents, whether they are published or not. The documents may come from teaching and research institutions in France or abroad, or from public or private research centers.

L'archive ouverte pluridisciplinaire **HAL**, est destinée au dépôt et à la diffusion de documents scientifiques de niveau recherche, publiés ou non, émanant des établissements d'enseignement et de recherche français ou étrangers, des laboratoires publics ou privés.

ORIGINAL RESEARCH

Ageing evaluation of cable insulations subjected to radiation ageing: Application of principal component analyses to Fourier Transform Infra-Red and dielectric spectroscopy

Simone Vincenzo Suraci¹  | Sandrine Amat² | Lea Hippolyte² | Astrid Malechaux² |
Davide Fabiani¹  | Claire Le Gall³ | Océane Juan³ | Nathalie Dupuy²

¹LIMES, Department of Electrical, Electronic and Information Engineering, University of Bologna, Bologna, Italy

²Aix Marseille University, Avignon Université, CNRS, Marseille, France

³Institut de Radioprotection et de Sécurité Nucléaire, Marseille, France

Correspondence

Simone Vincenzo Suraci, LIMES, Department of Electrical, Electronic and Information Engineering, University of Bologna, Bologna, Italy.
Email: simone.suraci@unibo.it

Nathalie Dupuy, Aix Marseille University, Avignon Université, CNRS, IRD, IMBE, Marseille, France.
Email: nathalie.dupuy@univ-amu.fr

Associate Editor: Chuanyang Li

Funding information

H2020 Euratom, Grant/Award Number: 755183

Abstract

The evolution of properties of crosslinked polyethylene (XLPE)-based insulating materials under radio-chemical ageing conditions is presented and discussed. In total, seven different polymer compounds were tested, characterised by an increasing quantity of additives, for example, antioxidants (AOs) and fillers as flame retardants. Samples were analysed using different testing techniques, that is, Fourier Transform Infra-Red and dielectric spectroscopy. This allowed a broad characterisation of the polymer, bringing to good correlations between the arising of new chemical groups caused by ageing and the modifications on the complex permittivity. Phenol-based AOs are found to be the most efficient in terms of protection against oxidation. On the contrary, flame retardants are concluded not to have any impact on the material ageing. Acquired data were then treated using the principal component analysis. The data treatment successfully distinguished the material composition (with and without additives) and the ageing environments. The results confirm the relevance of this analysis in understanding the impact of irradiation on the chemical and functional properties of the polymer materials studied.

1 | INTRODUCTION

The Paris Agreement, signed in 2015, aims at keeping the increase of global temperature below 2°C, preferably under 1.5°C, compared to pre-industrial levels [1]. This ambitious aim is hindered by, among other factors, the increasing energy demand. As a matter of fact, the most impacting activity causing climate change and the increase of global temperature is due to energy production. For this reason, various zero-carbon or low-carbon energy systems, that is, wind turbines and photovoltaic panels, experienced a huge and fast development in the last decades. Besides being protagonists of the desired energy transition, these energy sources are not sufficient for efficiently addressing the mentioned energy

demand. The reason for that is mainly twofold. On one hand, the energy sources are intermittent and not constantly available. On the other hand, to obtain significant installed power, they need large space, which is often not available in urbanised areas.

Furthermore, the carbon footprint of these systems is not zero. The Intergovernmental Panel on Climate Change [2] estimated that solar and wind energy sources release, respectively, 27 and 12 gCO₂ equivalent per produced kWh (Figure 1).

Indeed, while these systems do not produce CO₂ during their operation, the procedures for extracting raw materials, system production, and installation practices can emit significant quantities of CO₂.

This is an open access article under the terms of the Creative Commons Attribution-NonCommercial License, which permits use, distribution and reproduction in any medium, provided the original work is properly cited and is not used for commercial purposes.

© 2022 The Authors. *High Voltage* published by John Wiley & Sons Ltd on behalf of The Institution of Engineering and Technology and China Electric Power Research Institute.

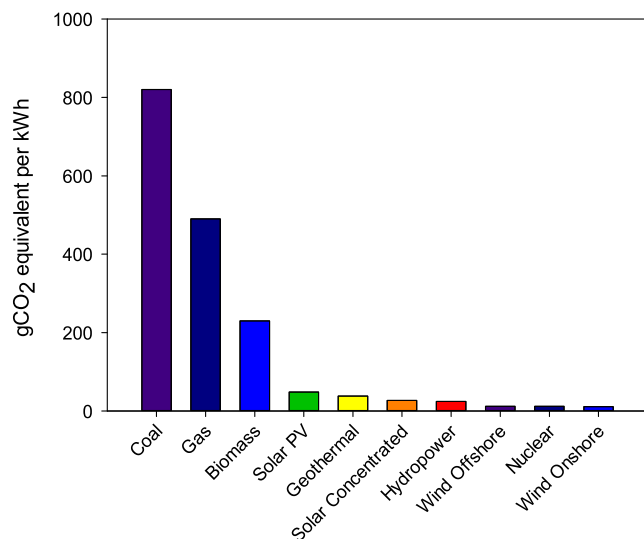


FIGURE 1 Average life-cycle carbon dioxide-equivalent emissions for different electricity generators (Source: Intergovernmental Panel on Climate Change (IPCC))

From Figure 1, it is possible to notice how nuclear power has a very low emission factor (12 gCO₂ equivalent per produced kWh), the same as offshore wind turbines. Energy production from nuclear reactors does not produce any CO₂ emission and, for this reason, it is considered as a clean and low-carbon energy source. Nuclear energy permits the overcoming of the limitations of the current renewable power systems, delivering a very high quantity of energy at any time. As an example, installed power in modern reactors may go beyond 1 GW as in the case of the newly operating Finland Olkiluoto reactor (1.6 GW). Thus, the unavailability of such big power may bring to very significant problems. As a consequence, reliability of the entire equipment involved in the nuclear power plants (NPPs) must be very high and continuously monitored to avoid any accident, system failure, and sudden power unavailability to the grid.

Existing NPPs started their operation during the 70s and 80s and they are now approaching their end-of-life (EoL), designed to be around 40 years. Given the big impact of NPPs on current energy production, NPP operators wish to extend the plant operation life to other 20 years. To do so, all the equipment and components inside the plants need to be verified and their status should be assessed to be in good condition. Among the numerous components, low voltage (LV) cables are very significant in terms of both quantity and associated role [3–6].

Low voltage cables are widely used inside NPPs for delivering signals (instrumentation and control (I&C) cables) and energy (power cables) [7]. Depending on where these cables are placed, for example, inside or outside the containment area, close to valves, etc., different safety requirements are mandatory. In particular, the most common categorization for these cables distinguishes among cables inside the containment vessel with and without the need to work after a nuclear accident (K1 and K2, respectively) and outside the

containment vessel (K3). Given the large quantity and high safety standards of these cables, the continuous condition monitoring is highly recommended, and a key issue is still not properly addressed [3, 7–10].

Performance of LV cables may deplete during their service time due to environmental stresses, for example, temperature and radiation, which may be high inside nuclear environments. In particular, the weakening of the insulation system, which is made up of polymeric materials, may cause the failure of the cable, leading to unavailability of important pieces of equipment, for example, safety-related one.

Current procedures [7, 11] assess the suitability of an LV cable to work in a nuclear environment if its elongation-at-break (EaB) is higher than 50% (absolute value). This value comes from a report issued by the Electrical Power Research Institute in early 2000s where several nuclear-scale cables were tested before and after a simulated loss of coolant accident (LOCA). It was verified that all the cables resisting the LOCA owned an EaB >50%, which was chosen as an end-of-life criterion. This mechanical criterion is very suitable for cable ageing assessment because the EaB property well follows the ageing evolution, and it guarantees the minimum mechanical properties required in real environments. Nonetheless, the use of this criterion is limited by the destructiveness of the testing technique, and consequently, the impracticality to continuously monitor the cable conditions.

Thus, in recent years, various monitoring techniques have started being proposed aiming to overcome these issues. On one hand, physical-chemical techniques require very small part of the cable insulation (microsampling) for a correct analysis of the ageing state of the cable system. Therefore, these techniques can be considered as quasi-nondestructive ones. On the other hand, electrical techniques are fully nondestructive techniques, and they can be performed onsite, providing useful insights on the cable-insulating properties and their variation with ageing [9, 12–17].

As an example, Fourier Transform Infra-Red (FTIR) spectroscopy is a localized technique, and very little samples are required to properly perform the analysis. It permits the evaluation of the chemical groups inside the polymer and consequently of the products coming from polymer ageing, for example, oxidized polymer chains. The possibility to quantify the oxidation inside the samples also allows the assessment of the expected cable lifetime once the end-of-life criterion is set [18]. As a drawback, in real conditions, the microsampling can be done only close to the cable terminations, which may not be representative of the entire cable, which usually passes across different environments, resulting into differently aged cable sections.

With reference to the electrical techniques, dielectric spectroscopy (DS) is gaining more and more interest in recent years [13, 15–17, 19–22]. This technique measures the polarization of the insulating material under an applied electric field. The reference quantity, the complex permittivity, was demonstrated to properly follow the ageing evolution of the insulation system [9, 13, 14, 22]. In addition, the technique is completely non-destructive, and the measurements are referred to the

entire cable length since the voltage is applied through the inner conductor, which is accessible through the cable terminations [9].

Nowadays, various works have already presented the consistency between the variation of the abovementioned tested quantities with the ageing development for various common polymeric materials [13, 17, 19, 21–26]. Nonetheless, this huge amount of data was not properly investigated through in-depth data analysis techniques such as the principal component analysis (PCA). This technique showed in various works [27, 28] to well identify and distinguish several parameters of interest, for example, the presence of substances and ageing level inside the polymer, without prior information on their chemical formulation.

In this work, the authors aim at presenting a broad characterization, through both chemical and electrical analyses, of polymeric materials used as insulators for LV cables and their behaviour with ageing. Investigated samples are characterized by a same crosslinked polyethylene (XLPE) matrix with an increasing quantity and complexity of antioxidants (AOs) and fillers. Analyses on these materials would permit to recognize the contribution of these additives on the ageing evolution by correlation with experimental data. Obtained data are then analysed through the Principal component analysis (PCA) technique to highlight the role of various parameters, which may modify the polymer properties with ageing, for example, additives, absorbed dose, and dose rate.

2 | MATERIALS AND METHODS

2.1 | Materials and ageing

The compositions of the seven model materials used in this study are given in Table 1. They were manufactured as thin tapes (0.5 mm thick) and based on silane XLPE as described in [28]. Polyethylene crosslinked by means of silanes (Si-XLPE) is widely used as an insulator for LV cables due to its easy processability and low-cost manufacturing process. In particular, the crosslinking phase does not involve any dicumyl peroxides and no crosslinking by-products are produced during the process. Two types of AOs were used in Mod2, 3, 4, and 7: Irganox 1076, inhibiting the propagation of free radicals and Irganox PS 802, blocking the formation of hydroperoxides mainly in case of thermal ageing. Moreover, one flame retardant (Alumina Tri-Hydrate (ATH)) was added to Mod5, 6, and 7. The impact of these additives on the ageing behaviour of XLPE has been studied in three radio-oxidant conditions close to room temperature (low, medium, and high dose rates). The corresponding accelerated ageing treatments took place in ÚJV (Řež, Czech Republic). The tapes were placed in a metallic cylinder in the irradiator (Panoza for low and medium dose rates or Roza for high dose rate) and maintained at constant temperature. The samples were turned over every 3 weeks to ensure the homogeneous integrated dose in the whole sample and withdrawals took place at constant time interval. Ageing condition specifications are reported in Table 2.

TABLE 1 Description of the compositions the different samples studied. %_w represents the percentage in weight of the additive and/or filler in the matrix

Name	Si-XLPE	Irganox 1076	Irganox PS802	ATH
Mod1	100% _w	–	–	–
Mod2	99% _w	1% _w	–	–
Mod3	99% _w	–	1% _w	–
Mod4	98% _w	1% _w	1% _w	–
Mod5	83% _w	–	–	17% _w
Mod6	67% _w	–	–	33% _w
Mod7	65.8% _w	0.7% _w	0.7% _w	32.8% _w

2.2 | Fourier Transform Infra-Red spectroscopy

FTIR spectra were collected in an Attenuated Total Reflectance (ATR) mode in the mid-IR domain (400–4000 cm^{−1}) using a Nicolet IS50 FTIR spectrometer equipped with a monolithic diamond crystal provided by Thermo-Fisher Scientific.

A background spectrum was first acquired in ambient conditions and subtracted to each sample spectrum. During data collection, the samples were simply clamped in contact to the ATR crystal. A hundred scans were then performed and averaged leading to a spectral resolution of 4 cm^{−1} for the final experimental spectra. Three spectra were collected at three different locations on each sample to differentiate intrinsic samples inhomogeneity from ageing-induced chemical modifications.

2.3 | Dielectric spectroscopy

Permittivity of investigated materials was obtained through a Novocontrol Alpha dielectric analyser v2.2. Permittivity $\hat{\epsilon}$, as a complex quantity, can be written as follows:

$$\hat{\epsilon} = \epsilon' - j\epsilon'' \quad (1)$$

where ϵ' is the real part of permittivity related to the energy stored in the material, and ϵ'' is the imaginary part of permittivity related to the dielectric losses of the material.

The device operates at 3 V in the frequency region 10^{−2}–10⁶ Hz. The considered frequencies allow the evaluation of dipolar polarization for frequencies higher than 10⁴ Hz. On the contrary, lower frequencies are mainly related to interfacial polarization and movements of charge carriers due to conduction mechanisms. Measurements were conducted at room temperature for all the considered materials and ageing conditions.

Among these frequencies, it was chosen to report, in the result section, the trend of complex permittivity at 100 kHz. Though, the entire dielectric spectrum is used for the PCA data analyses. The considered frequency (100 kHz) was found to be a good marker for the assessment of polymer ageing [13–15, 29].

TABLE 2 Accelerated ageing conditions

Ageing condition	Dose rate (Gy h ⁻¹)	Temperature (°C)	Withdrawal dose (kGy)	Max. aged dose (kGy)
Low dose rate	8.5	47	~24	~138
Medium dose rate	77.8	47	~67	~374
High dose rate	400	21	~67	~336
Combined ageing	8.5	87	~24	~138

The reason for that is found on the dipolar polarization mechanism occurring in that frequency region. Indeed, the degradation products coming from polymer ageing are characterised by a permanent dipole whose estimated moment can reach values up to 3 Debyes. The presence of dipoles modifies the material behaviour once an electric field is applied, leading to an increase of dielectric losses in the frequency region related to the dipolar polarization (10^3 – 10^9 Hz) [30]. In addition, DS is a quantitative technique allowing the correlation of the amplitude of the peak with the concentration of dipolar species inside the material as it will be discussed in the following section.

2.4 | Principal component analysis for data treatment

PCA is a tool commonly used in chemometrics and it was described in a previous study [28, 31]. The principal component analysis is an unsupervised modelling method, also known as the projection method, and it is often the first step in the exploratory data analysis aiming to find patterns in the data. The procedure establishes a linear spectral model, which allows original and correlated variables to be converted into uncorrelated variables called principal components or loadings. These latent variables contain the main information and are calculated from data differences and similarities. The procedure also reduces data with no information loss: generally, a small number of principal components (PCs) is sufficient to summarise the available information. The principal component analysis is oriented towards modelling the variance/covariance structure of the data matrix into a model, which is based on the significant data differences (significant scores) and considers noise as an error. The number of principal components depends on the model complexity. Generally, the first component extracts the largest source of variance and the last one only extracts noise. For infrared spectra, the spectral range 1800–670 cm⁻¹ was used for chemometrics treatment and it corresponds to 588 numerical points.

3 | EXPERIMENTAL RESULTS AND DATA ANALYSES

3.1 | Fourier Transform Infra-Red results

In this section, results coming from FTIR-ATR measurements as well as related PCA are reported. Due to the significant

number of different polymer compounds, it was chosen to report experimental results related to the neat XLPE (Mod1), XLPE stabilised with AOs only (Mod2, 3, and 4), and the full stabilised XLPE (Mod7). On the contrary, the full set of data will be used for the PCA data treatment.

3.1.1 | Experimental results and discussion

For easier comparison of the different samples, the FTIR-ATR spectra presented in this section have been normalised by the intensity of the band located at 1472 cm⁻¹ (δ -CH₂ deformation in the plane), which are considered as an internal standard (not affected by the ageing conditions). A focus on the hydroxyl zone extended up to 2900 cm⁻¹ (3800–2900 cm⁻¹), carbonyl (1850–1600 cm⁻¹), and ester regions (1500–900 cm⁻¹) was made to highlight the changes occurring in the samples during ageing. A recap of the main IR bands observed in the different tapes is shown in Table 3.

FTIR-ATR spectra for unaged Mod1, 5, and 6 exhibit the same absorption bands exception given for the signal attributed to ATH visible both in the hydroxyl (3619–3372 cm⁻¹) and ester (1020–912 cm⁻¹) regions of Mod5 and 6 (Figure 2). A/A (1472) is the ratio between the absorbance of the considered peak and the absorbance of the peak at 1472 cm⁻¹ (reference peak). The signal of ATH does not evolve with irradiation time whatever the dose rate and temperature. In these three unaged samples, no additional absorption band can be observed in the carbonyl region nor the hydroxyl region. In the first period of irradiation, for every dose rate, absorption bands appear in the carbonyl zone at 1733 and 1712 cm⁻¹ (as shown in Figure 3 for Mod1) correlated with the appearance of peak at 932 cm⁻¹ in the ester zone (Figure 2 for Mod1). These bands can only be attributed to oxidation products of XLPE (carboxylic acids and esters in this case as ATH is not supposed to react in the tested conditions). Two broader bands attributed to γ -lactones and vinylenes appear later at 1770 and 1625 cm⁻¹, respectively (from 389 days of irradiation at low dose rate and 125 days at medium dose rate). These two bands are correlated with the ones observed at 1408 and 1284 cm⁻¹, respectively. The signal of oxidation products is higher at medium and low dose rates compared to high dose rates. These observations highlight that the clear degradation of XLPE under gamma irradiation and that radio-oxidation is less damaging for pure XLPE at a high dose rate. Indeed, at 400 Gy h⁻¹, dissolved oxygen is being consumed faster than at 8.5 Gy h⁻¹ and 77 Gy h⁻¹. Then, it is possible to suppose that the permeation of atmospheric oxygen may not be efficient

TABLE 3 Main IR bands observed in the samples and their evolution after ageing ((+) increase of intensity (−) decrease of intensity (0) no change)

Samples	Wavenumber (cm ^{−1})	Type of vibration	Evolution with ageing	Ref.
Unaged XLPE	2919, 2883	ν -(CH ₂) stretching asymmetric	(0)	[36]
	2851, 2848	ν -(CH ₂) stretching symmetric		
	1472 and 1462	δ -(CH ₂) deformation in the plane (amorphous and crystalline)	(0)	
	1367 and 1352	γ -(CH ₂) wagging (amorphous and crystalline)	(0)	
	1379	δ -(CH ₃) bending (amorphous)	(0)	
	1087	ν -(CH ₂) rocking amorphous (theoretically at 1078 cm ^{−1})	(−)	
	1020	γ -(CH ₂) rocking crystalline (theoretically at 1050 cm ^{−1})	(−)	
	728–719	δ -(CH ₂) deformation in the plane (crystalline)	(0)	
ATH	3619, 3524, 3436, 3392, 3371	ν -(Al-OH) OH stretching	(0)	[37, 38]
	1020, 966 and 914	(Al-OH) OH bending		
	792	ν -(Al-O) stretching		
AO (Irganox 1076 and PS802)	3639	ν -(OH) stretching of phenol (Irganox 1076)	(−)	[32, 33]
	2954	ν -(CH ₂ -S) CH ₂ asymmetric stretching (Irganox PS 802)	(0)	
	1743, 1733	ν -(C=O) stretching of ester (Irganox 1076 and PS 802)	(−)	
	1394	ν -(C-O) stretching of ester (Irganox 1076 and PS 802)	(0)	
	1364	C-OH bending (Irganox 1076)	(0)	
	1240	ν -(C-O) asymmetric stretching (Irganox PS 802)	(+)	
	1178	ν -(C-O) stretching of phenol (Irganox 1076)	(+)	
	1170	ν -(C-O) stretching of ester (Irganox PS 802)	(−)	
	1275–1185, 1160–1050	ν -(C-O-C) stretching of ester asymmetric symmetric (Irganox 1076 and PS 802)	(+)	
	869	δ -(CH) bending of aromatic (Irganox 1076)	(0)	
Oxidation products	1770	ν -(C=O) stretching	(+)	[40]
	1734–1735	γ -lactones, esters (aliphatic saturated)		
	1733	Saturated aldehydes		
	1720–1724	Ketones		
	1710–1714	Carboxylic acids		
	1625, 1284	ν -(C=C) stretching (phenolic unsaturations)	(+)	
	1408	ν -(CO-CH ₃) asymmetric vibration or ν -(CO-CH ₂) symmetric vibration of ketones	(+)	
	1170	γ -(CH ₂) rocking amorphous		
	1105	ν -(C-CO-C) asymmetric stretching of ketones	(+)	
	1417	ν -(C-O) stretching of aromatic ketones	(+)	
	1313, 1261, 1130	γ -(C-CO-C) asymmetric stretching of ketones	(+) then (−)	
	1180	ν -(C-O) stretching of ketones	(+)	
	988, 932	δ -(OH) bending of aromatic carboxylic acids	(+) then (−)	
	1720	3,3 thiodipropionic acid	(+)	
	1363	ν -(C=O) stretching		
	1311–1263	ω -CH ₂ -S wagging, δ -(O-H)		
	1234	ν = C-O asymmetric stretching		
	1187	δ -(O-H) and ν -(C-O) combination		
	1130	ν -(C-O) stretching		

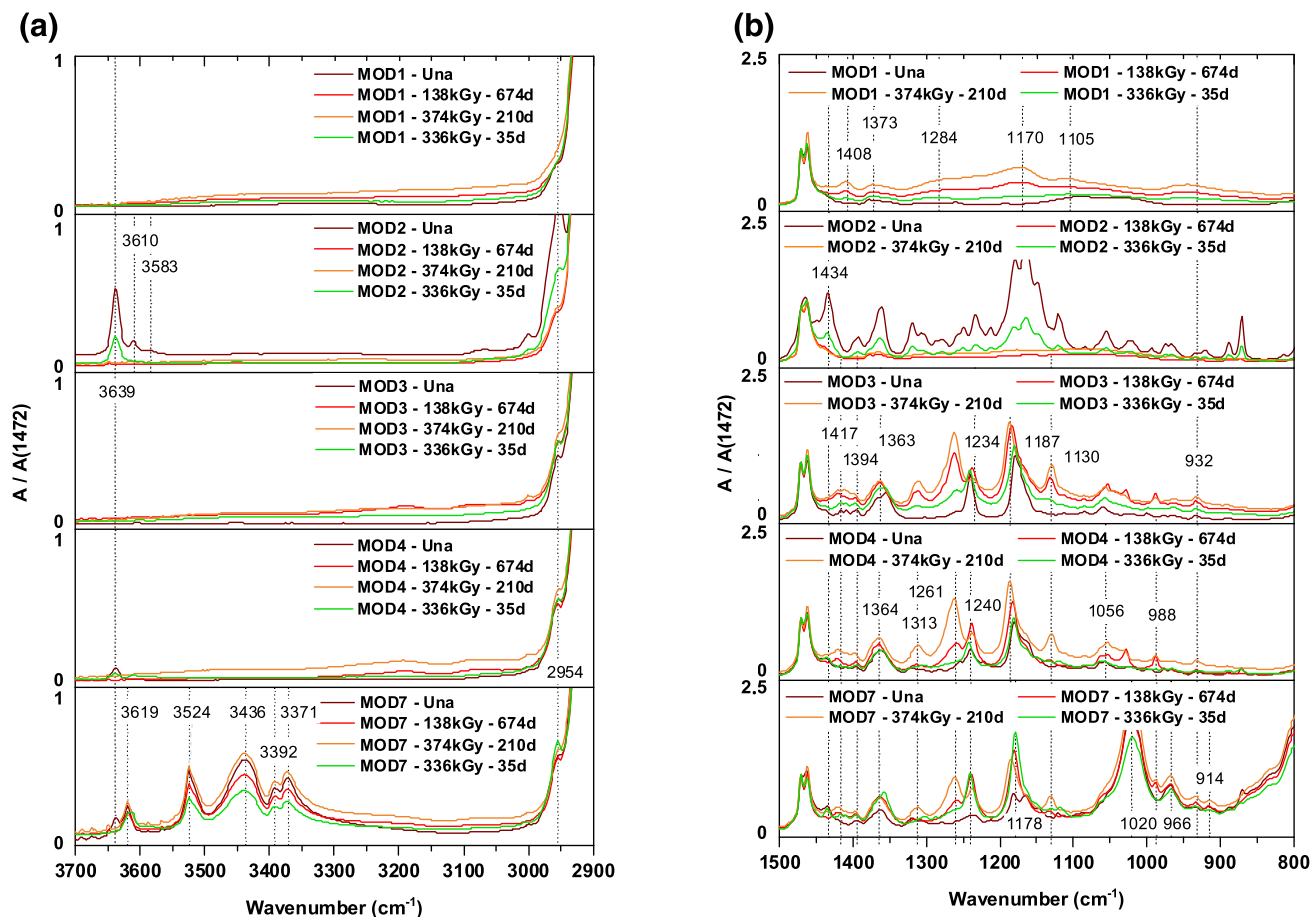


FIGURE 2 Extended hydroxyl (a) and ester (b) regions of FTIR-ATR spectra of Mod1, 2, 3, 4, and 7 (top to bottom) unaged samples, radiolytically aged at the highest dose obtained at a low dose rate (8.5 Gy h^{-1} , 47°C), a medium dose rate (77.8 Gy h^{-1} , 47°C), and a high dose rate (400 Gy h^{-1} , 21°C)

due to the high consumption pace at high dose rates, leading to the diffusion limited oxidation (DLO). At 8.5 Gy h^{-1} , the oxidation may permeate more easily into the sample. As a matter of fact, longer ageing times enhance the chance for the radicals to react with oxygen, leading to the arising of degradation species, for example, carboxylic acid, ketones, aldehydes, etc.

Unaged Mod2 and 3 spectra exhibit additional absorption bands compared to Mod1, related to the presence of Irganox 1076 and Irganox PS 802, respectively. Notably, in Mod2 (Figure 2), three peaks at 3639, 3610, and 3583 cm^{-1} are visible in the hydroxyl zone. These may be related to the presence of Irganox 1076 under forms I, II, and III [32, 33]. One peak at 1733 cm^{-1} in the carbonyl region is associated with form I and a wide range of peaks in the ester one (between 1000 and 1400 cm^{-1}) may be related to the different forms. In Mod3, no band is observed in the hydroxyl region, but a wide range of new bands are present in the ester one (between 1000 and 1400 cm^{-1}) as well as two peaks in the carbonyl region at 1733 and 1743 cm^{-1} (ester groups of Irganox PS 802).

During irradiation at low and medium dose rates, the principal changes occur in the carboxyl and hydroxyl zones. Indeed, the three initial bands in the Mod2 hydroxyl zone disappear. Moreover, the peak observed in the carbonyl region

of Mod2 spectrum is shifted towards lower wave numbers (1726 then 1716 cm^{-1}) corresponding to ketones and carboxylic acids and other bands appear at 1737 , 1770 , and 1627 cm^{-1} (ester and γ -lactones groups and phenolic unsaturations, respectively). These band positions differ from Mod1 showing that Irganox 1076 has a stabilising effect in radio-oxidant conditions. Concerning Mod3, the band present at 1743 cm^{-1} is shifted to 1739 cm^{-1} and the one at 1733 cm^{-1} is shifted to 1731 cm^{-1} . Moreover, two peaks appear at 1720 and 1712 cm^{-1} showing the formation of ketones and carboxylic acids, respectively. Mod3 then behaves as Mod1 showing that Irganox PS 802 is not efficient in these conditions. Indeed, the effect of primary AOs (Irganox 1076) is to interrupt the oxidative degradation reaction chain by scavenging the radicals caused by the environmental stresses. On the contrary, secondary AOs (Irganox PS802) react with products coming from the degradation of primary AOs. So that, their protection effect may be seen only when the two AOs are used in combination leading to a synergistic inhibition effect.

At a higher dose rate, changes in Mod2 and 3 spectra occur in a less extent, confirming the reduced impact of oxidation in these conditions, similar to Mod1, 5, and 6.

The observations performed on Mod2 highlight the consumption of Irganox 1076 during gamma irradiation. Dorey

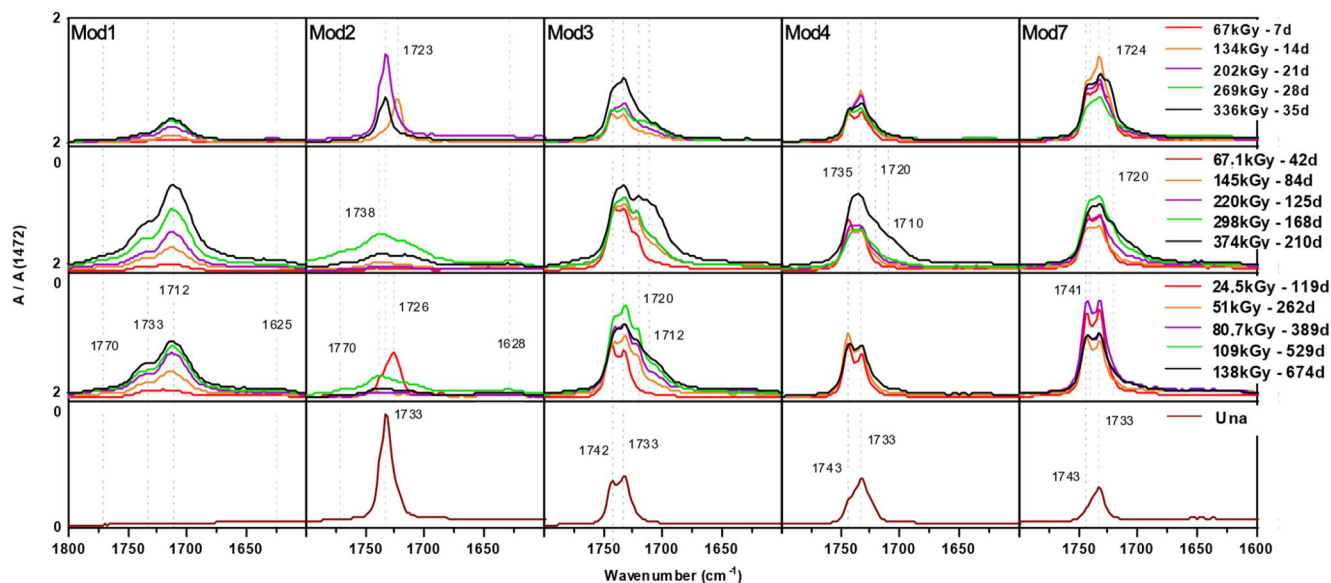


FIGURE 3 Carbonyl region of FTIR-ATR spectra of investigated samples. From bottom to top: unaged sample, radiolytically aged at a low dose rate (8.5 Gy h^{-1} , 47°C), at a medium dose rate (77.8 Gy h^{-1} , 47°C), and a high dose rate (400 Gy h^{-1} , 21°C)

et al. [34] described the complex formation mechanisms leading to degradation products, which results into an IR spectrum with hardly identifiable bands except for the ones of XLPE. The observations made on Mod3 suggest a significant chemical consumption of Irganox PS 802 during gamma irradiation. This phenomenon was not observed in the case of thermal degradation, since physical loss by evaporation is considered to be the main ageing process [35]. The expected oxidation product is the 3,3'-thiodipropionic acid, whose characteristic bands are observed in aged Mod3 spectra at 1720 cm^{-1} , 1363 cm^{-1} , 1311 cm^{-1} to 1263 cm^{-1} , 1234 cm^{-1} , 1187 cm^{-1} , and 1130 cm^{-1} (Figure 2).

Unaged Mod4 and Mod 7 spectra are very close to each other, and they are a mixture between Mod2 and 3 signals. Only one band at 3639 cm^{-1} out of three visible in Mod2 is observed in the hydroxyl zone of Mod4 and 7, which indicates that Irganox 1076 is only present in its polymorphic form I. Alumina Tri-Hydrate bands are again observed in the hydroxyl and ester regions of Mod7 spectrum as it is the case for Mod5 and 6. One peak is visible in the carbonyl zone at 1733 cm^{-1} with a shoulder located at 1743 cm^{-1} , which is the sign of both Irganox 1076 and Irganox PS 802.

During radio-oxidative ageing (at low and high dose rates), the peak at 1743 cm^{-1} is shifted towards a lower wave number (at 1741 cm^{-1}), and the relative absorbance of the doublet is reversed (Figure 3 for Mod4 and Mod7). For the highest dose obtained at a medium dose rate, these bands result to be broader. In addition, a broad peak centred at 1735 cm^{-1} with two shoulders at 1720 and 1710 cm^{-1} appears corresponding to the formation of ketones and carboxylic acids. In the hydroxyl region (Figure 2), the band observed at 3639 cm^{-1} rapidly disappears with irradiation as for Mod2.

The following main conclusions can be inferred from the different observations described in this section:

- High dose rate induces less degradation of XLPE and stabilised XLPE because of DLO.
- Irganox 1076 has an efficient stabilising effect towards radio-oxidation of XLPE whether used alone or in association with Irganox PS 802.
- Irganox PS 802 has been consumed under radio-oxidant conditions at room temperature, but this phenomenon did not result in any stabilisation of XLPE.
- ATH is not impacted by radio-oxidation and has no effect at all on XLPE degradation in these conditions.

3.1.2 | Principal component analyses on Fourier Transform Infra-Red

(1) General analyses on a complete dataset

In Figure 4, the two first principal components represent 91% of the total variance included in the spectra. The scores show one group with Mod1, Mod2, Mod3, and Mod4 on the negative part of PC1 and Mod5, Mod6, and Mod7 are regrouping in the positive part of PC1. The different groups are explained by the composition of each model according to the presence of additives and their concentration. In the following, PCAs is presented and discussed per each model.

(2) Mod1 (XLPE without additives)

Figure 5 reports the PCA scores and loadings for Mod1. The PC1 represents 94% of the total variance. Since the non-irradiated samples are negatively projected, it may be possible to highlight that all the aged samples with negative score are very limitedly impacted by ageing. As the scores attributed to the high dose rate are all negative, we conclude that the impact

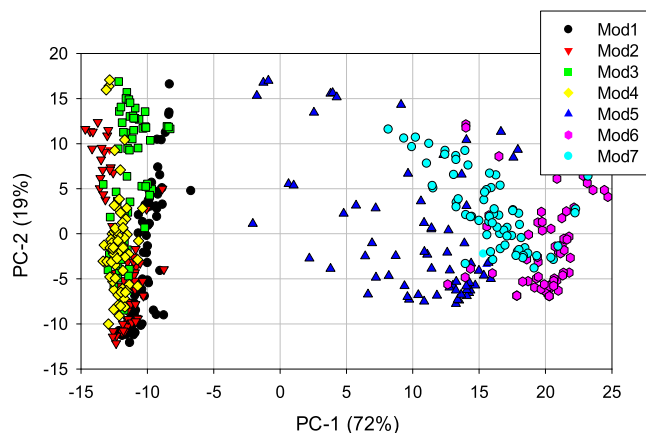


FIGURE 4 Principal component analysis (PCA) results for all the models on infrared spectra. PC-1 and PC-2 are first and second principal components, respectively

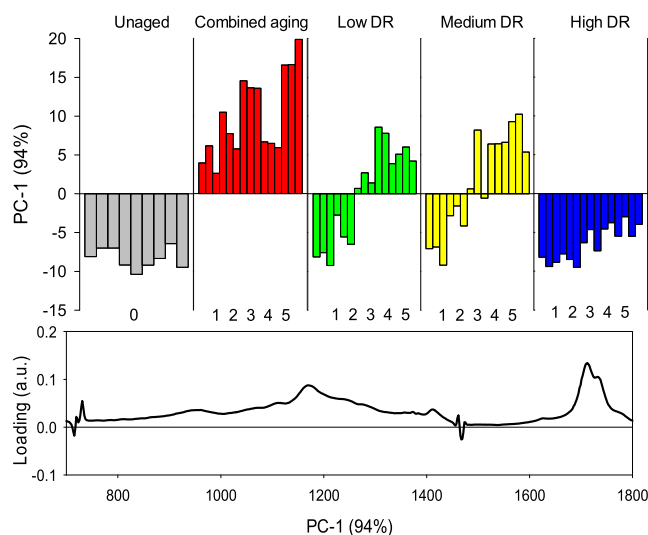


FIGURE 5 Principal component analysis (PCA) scores (top), Fourier Transform Infra-Red (FTIR) spectra for all doses and PCA loadings (bottom) of the PC-1 for the analysis of Mod1. X-axis: 0–5 ageing levels. Three measurements per each ageing level on aged samples

of gamma irradiation is less important at 400 Gy h^{-1} than for lower dose rates as discussed for FTIR analyses in the previous section. For 8.5 and 77 Gy h^{-1} ageing at room temperature, the scores increase with the dose from negative to positive values (up to 51 kGy). Finally, it can be noticed that the loading associated with PC1 is linked to the absorbed dose and correlated with carbonyl band intensity.

(3) Mod2 (XLPE (99%_{w/w}) with Irganox 1076 (1%_{w/w}))

With reference to Mod2 PC analyses, Figure 6 reports that the PC1 explains 85% of the total variance. The scores associated with the first component reveal that the impact of gamma irradiation is, also in this case, less significant for the high dose rate than for the low and medium ones (Figure 6).

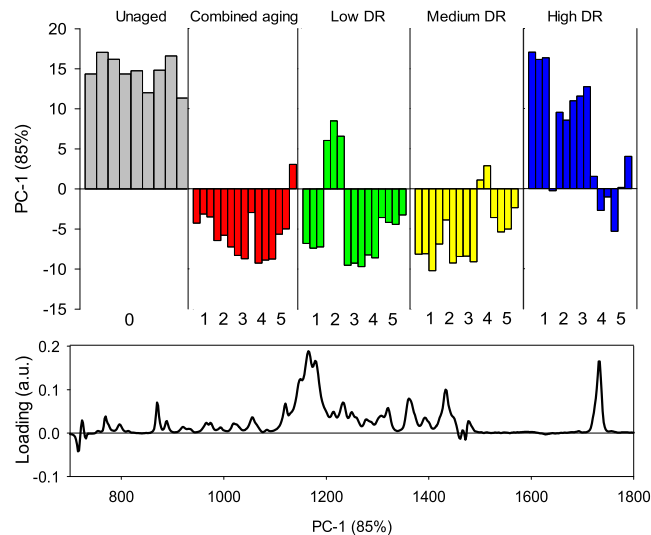


FIGURE 6 Principal component analysis (PCA) scores (top), Fourier Transform Infra-Red (FTIR) spectra for all doses and PCA loadings (bottom) of the PC-1 for the analysis of Mod2. X-axis: 0–5 ageing levels. Three measurements per each ageing level on aged samples

For the 400 Gy h^{-1} ageing, the impact of irradiation is correlated to the dose, even if the impact of the modification is not homogenous [28]. The loading chart shows positive bands, which could be attributed to Irganox 1076 (Table 3). In the negative part of the loadings, the two bands at 1471 and 715 cm^{-1} are again attributed to the XLPE polymer (Table 3). Firstly, the consumption of Irganox 1076 increases with the dose received at 400 Gy h^{-1} , whereas a strong consumption occurs at low and medium dose rates regardless of the dose. Secondly, physical loss of additives can occur by a blooming effect [28, 33]. Thus, a combination of physical loss and chemical degradation of the additive should be considered as discussed in Section 3.1.1.

(4) Mod3 (XLPE (99%_{w/w}) with Irganox PS802 (1%_{w/w}))

Regarding Mod 3 PCA (Figure 7), the two first principal components represent 83% of the total variance. The scores associated with the first component indicate that the impact of gamma irradiation is, also in this case, less important for the highest dose rate rather than for the 8.5 and 77 Gy h^{-1} dose rates. For the dose rate at 8.5 Gy h^{-1} , the radiolytic ageing starts quickly at 87°C and at 51 kGy at room temperature (21°C). For the high dose rate ageing, no degradation of the polymer is visible until 336 kGy . Then, PCA shows that the Irganox PS 802 is consumed according to the dose at 400 Gy h^{-1} and it is consumed independently of the dose at 8.5 Gy h^{-1} and 77 Gy h^{-1} .

(5) Mod4 (XLPE (98%_{w/w}) with Irganox 1076 (1%_{w/w}) and Irganox PS802 (1%_{w/w}))

Figure 8 reports the PCA results for Mod4. PC1 explains 78% of the total variance. The samples irradiated at 8.5 Gy h^{-1}

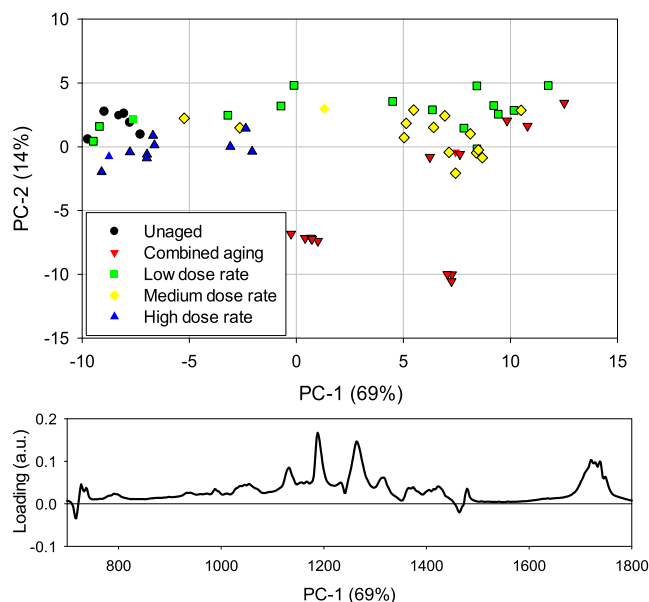


FIGURE 7 Principal component analysis (PCA) scores (top), Fourier Transform Infra-Red (FTIR) spectra for all doses and PCA loadings (bottom) of the PC-1 for the analysis of Mod3

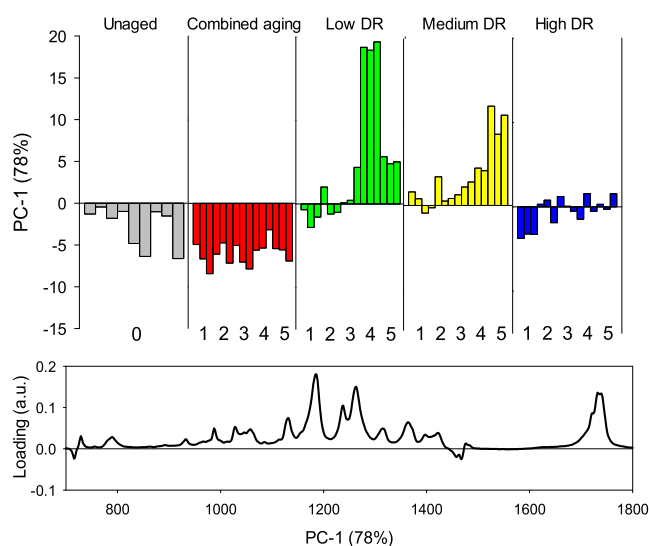


FIGURE 8 Principal component analysis (PCA) scores (top), Fourier Transform Infra-Red (FTIR) spectra for all doses and PCA loadings (bottom) of the PC-1 for the analysis of Mod4. X-axis: 0–5 ageing levels. Three measurements per each ageing level on aged samples

at 87°C exhibit negative PC1, suggesting a negligible degradation of the polymer. Indeed, thanks to a synergistic effect of Irganox 1076 and PS802, XLPE material is strongly protected from high temperatures. But at room temperature, the gamma-irradiation effect is the same as the one observed on the second formulation (XLPE + Irganox 1076). In this case, the scores (Figure 8) show that the impact of gamma irradiation is more significant in the case of lower dose rates. Regarding the medium dose rate, the degradation is incepted at 81 kGy and it increases with the dose, whereas for the 400 Gy h⁻¹ dose rate, the ageing effect is observed after 134 kGy. Then, it results

that, in the case of ageing temperatures close to ambient, there is no benefit associated with the presence of two additives in the polymer because results are very similar to those obtained with Irganox PS 802 only.

(6) Mod5 (XLPE (67%_{0w/w}) with ATH (33%_{w/w}))

Referring to Mod5 PC analyses (Figure 9), the two first PC represent 91% of the total variance. For 400 Gy h⁻¹, the sample does not seem to be impacted by irradiation and the impact of gamma irradiation is visible from 17 kGy dose for the 8.5 Gy h⁻¹ at 87°C, from 36 kGy for the 8.5 Gy h⁻¹ at room temperature, and from 67 kGy for the 77 Gy h⁻¹ ageing (Figure 9). After these doses, the oxidation may take place since the samples are separated on component one, but two groups can also be identified on the PC2. Gamma-irradiation induces the degradation of the polymer in particular with an increase of the carbonyl band ν-C=O at 1712 cm⁻¹ and change in the appearance of the vibration ν-C-O at 1170 cm⁻¹. Finally, it is worth noting that the ATH additive does not efficiently protect the XLPE polymer against radiolytic ageing, especially at the 77 Gy h⁻¹ dose rate, as already discussed in the FTIR-related section.

(7) Mod7 (XLPE (65.8%_{0w/w}) with ATH (32.8%_{w/w}), Irganox 1076 (0.7%_{w/w}), and Irganox PS802 (0.7%_{w/w}))

In the case of Mod7, the two first PCs represent 79% of the total variance. The impact of gamma irradiation is not visible until 51 kGy for the 8.5 Gy h⁻¹ ageing at room temperature and 298 kGy for the 77 Gy h⁻¹ ageing (Figure 10). For the highest dose rate, interpretation is more difficult due to a strong heterogeneity of the results. For the PC1, the impact of gamma irradiation is associated with a decrease of 1020 cm⁻¹ band principally attributed to the ATH additive (according to Table 3). Nonetheless, the synergistic effect of the two AOs is present, ensuring a high protection against degradation mechanisms. Thus, the XLPE polymer appears to be protected by the combination of the two Irganox additives and ATH fillers.

3.2 | Dielectric spectroscopy results

In this section, the results coming from DS measurements as well as their related PCA are reported. Due to the significant number of different polymer compounds, it was chosen to report experimental results related to the neat XLPE (Mod1), XLPE stabilised with AOs only (Mod4), and the full stabilised XLPE (Mod7). On the contrary, the full set of data will be used for the PCA data treatment.

3.2.1 | Experimental results and discussion

Figure 11 displays the complex permittivity as a function of ageing time and conditions for Mod1 (Figure 11a,b), Mod4

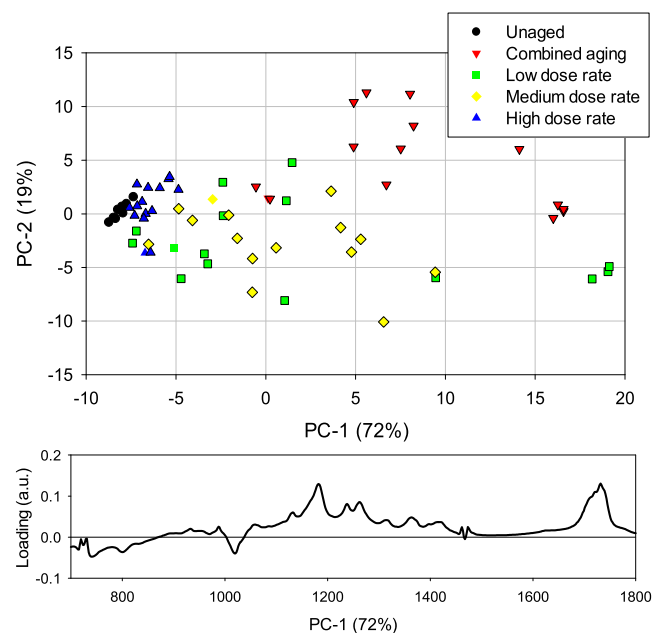


FIGURE 9 Principal component analysis (PCA) scores (top), Fourier Transform Infra-Red (FTIR) spectra for all doses and PCA loadings (bottom) of PC-1 for the analysis of Mod5

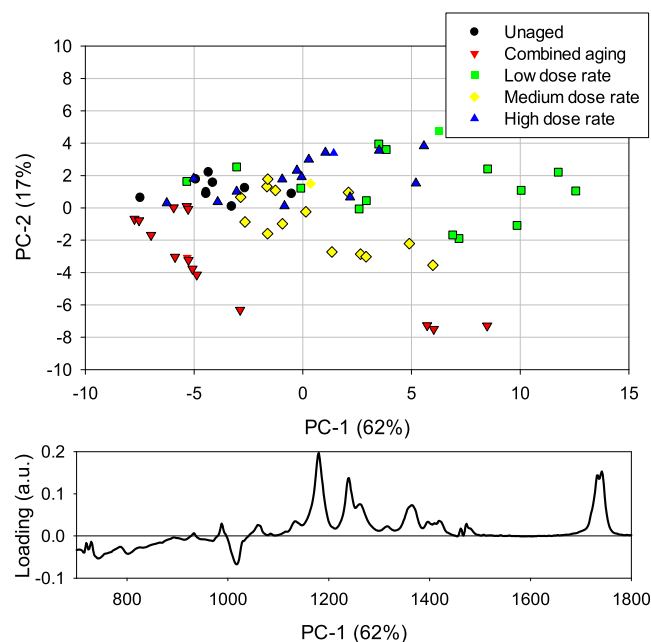


FIGURE 10 Principal component analysis (PCA) scores (top) and PC-1 loading (bottom) for Mod7

(Figure 11c,d), and Mod7 (Figure 11e,f) at 100 kHz. In all the considered cases, complex permittivity varies with ageing. However, its trend results to be significantly modified by the additives inside the different polymeric compounds [13, 42].

Referring to the neat polymer (Mod1), complex permittivity monotonously increases with ageing. This trend is expected since no external stabilizers (e.g., AOs) are present inside the polymeric compound as seen in [43, 44]. The absence of additional stabilizers allows the oxidative reactions to freely take place according to the well-known reaction scheme reported, for example, in [34, 45]. The degradation products arising with ageing are just given by the oxidation of the main polymer chain by substituting hydrogen atoms with oxidised groups, for example, ketones and carboxyl acids, as seen for the FTIR analyses. These species are highly polar, and, for this reason, they significantly impact the dielectric response, particularly at the analysed frequency value, leading to a large increase of the dielectric quantities (Figure 11a,b). Moreover, the slope of the increasing trend follows the ageing severity due to different degradation kinetics, confirming the good correlation between ageing development and growth of the property. In addition, it is worth noting how the increase of the dielectric property is limited in the case of highest dose rate, mimicking the behaviour already discussed with reference to the FTIR spectra (Figure 3) due to the DLO effect.

The addition of AOs (Mod4) modifies the trend of the property with ageing. During the first ageing periods, the variations of ϵ'' are very little and fluctuating around an average value (stabilisation phase). After a given time, which depends on the ageing severity, the property starts increasing to significantly high values (up to 10 times the value related to the unaged material), mimicking a plain XLPE trend. This

behaviour may be explained by the role of AOs. In particular, as already presented, in the initial phases of ageing, AOs protect the polymer from environmental oxygen. During this time, the increase of dipolar species due to ageing is limited, since only the conversion of AOs in their degradation products occurs. Once the conversion is completed and the AOs are consumed, oxidation reactions may take place (oxidation onset time). This leads to the arising of oxidised polymer chains, which, being strongly polar, enhance the dielectric response at the investigated frequencies (Mod1 behaviour).

The presence of ATH fillers (Mod7) causes the increase of the real part of permittivity for both unaged and aged polymers. In particular, the trend with ageing is very similar to the one just described for Mod4, but the real part of permittivity is shifted upwards by a factor of ~ 0.3 . The reason for that is probably related to the polar properties of the ATH molecules, which increase the dielectric response of the material throughout all the analysed frequencies. Similarly, the dielectric losses are also higher than in the case of unfilled materials (Mod1 and Mod4), bringing the imaginary part of permittivity for the unaged materials up to 0.013 from ~ 0.003 (Mod1). It is worth recalling at this point that, as reported in the previous section, ATH particles are inorganic species, so they have no impact on the degradation kinetics which is, on the contrary, led by AOs. As a further confirmation, also the trend of the dielectric losses with ageing is very similar to the one already described for Mod4. However, the results show that the increasing phase starts sooner than in the case of Mod4. This phenomenon may be assigned to the reduction of antioxidant protection by the ATH molecules. As seen in [13, 46, 47], ATH may deactivate by physical absorption the -OH group inside the phenolic

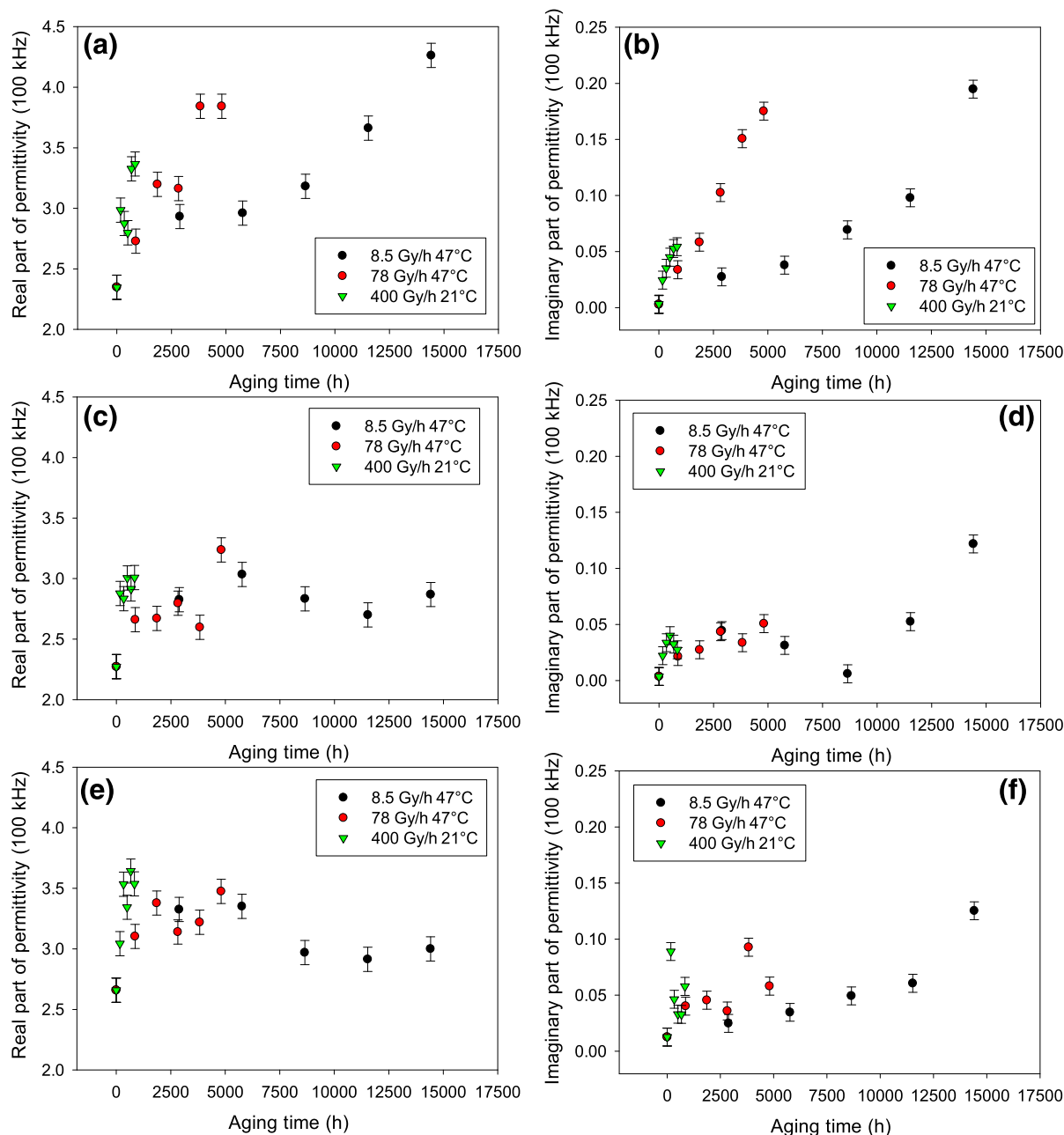


FIGURE 11 Real and imaginary parts of permittivity values at 100 kHz for the different analysed materials and ageing conditions. (a), (b) Mod1; (c), (d) Mod4; (e), (f) Mod7

antioxidant, hindering the diffusion of antioxidant in the polymer bulk and reducing its oxidative protection. As a result, the antioxidant kinetics results to be limited, leading to an earlier oxidation onsite time.

3.2.2 | Principal component analyses on dielectric spectroscopy

The principal component analysis was carried out to highlight the impact of film formulations and ageing on dielectric properties. In the following, PCA results are commented considering the different dose rates.

(1) High dose rate conditions

For the Mod1 to Mod7 on the high dose rate samples, the obtained PCA shows that the first principal component explains 89% of the total variance included in the data (Figure 12). The PCA separates samples based on the material (Mod1–4 vs. Mod5–7), highlighting the presence of ATH fillers. For Mod5, the ATH concentration is lower than for Mod6 and the intensity of scores is lower. There is no clear effect of the ageing on this result, but we can see that for the Mod5–7, the scores have higher ϵ'' values for frequencies below 100 Hz due to the interfacial polarization induced by interfaces of ATH fillers.

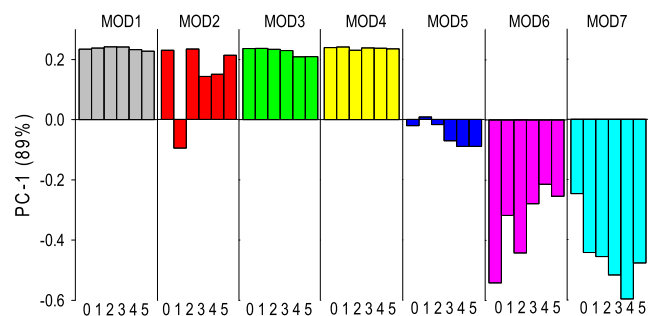


FIGURE 12 Principal component analysis (PCA) on ϵ'' for the high dose rate (Mod1 to Mod7). X-axis: 0–5 ageing levels

(2) Medium dose rate conditions

For medium dose rate samples, the obtained PCA (Figure 13) shows that 100% of the total variance is explained by the first principal component included in the data. Mod1, Mod3, Mod5, and Mod6 reveal a strong effect of ageing, especially for doses 4 and 5. Mod2, Mod4, and Mod7 do not exhibit the same behaviour probably due to the protective effect of Irganox 1076. The results on PC1 highlight the fact that degraded samples have higher values of ϵ'' for frequencies below 1 Hz.

(3) Low dose rate conditions

Concerning low dose rate ageing, the PCA in Figure 14 shows that the first principal component represents 98% of the total variance included in the data. There is an effect of ageing for Mod1, Mod3, Mod5, and Mod6 for high doses. On the contrary, polymers with AOs (Mod2, Mod4 and Mod7) depict lower values of PC being protected against oxidation due to the presence of Irganox 1076. We can also see that degraded samples have higher values of ϵ'' for frequencies below 1 Hz.

4 | CONCLUSIONS

In this article, a broad analysis on the ageing of PE-based materials with different additives and fillers was presented. It is found that ATR-FTIR and dielectric measurements give complementary and consistent information at different scales on radiolytic degradation of the studied material. In particular, even if the infrared investigations carried out by the ATR-FTIR analysis are based on the surface (first microns) of the samples, the results claim good accordance with the ageing occurring inside the polymer. Similarly, the trend of the dielectric property properly follows the ageing development, depicting different increasing trend slopes according to the ageing severity.

Through the data analysis, it is found that the dose rate is a determining factor rather than the dose itself, that is, the degradation is more important at low dose rates than at higher dose rates.

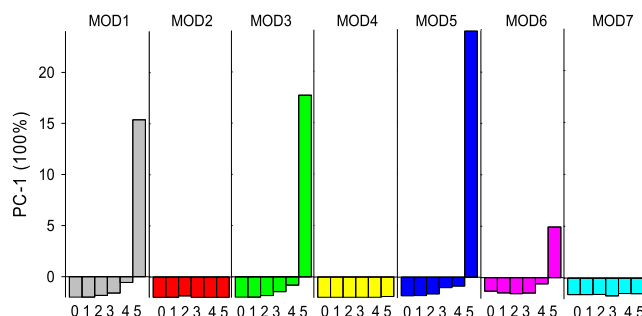


FIGURE 13 Principal component analysis (PCA) on ϵ'' for the medium dose rate (Mod1 to Mod7). X-axis: 0–5 ageing levels

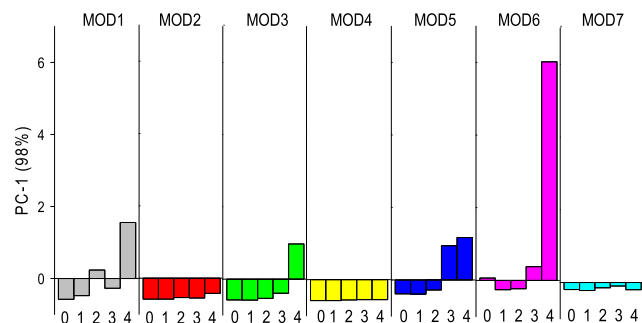


FIGURE 14 Principal component analysis (PCA) on ϵ'' for the low dose rate (Mod1 to Mod7). X-axis: 0–4 ageing levels

With reference to the impact of additives on the polymer properties, it was demonstrated that ATH fillers (Mod 5) do not modify the ageing evolution of the base polymer. Nonetheless, they modify the polar properties of the material, shifting upwards the complex permittivity trend with ageing.

On the contrary, the introduction of AOs limited the oxidative degradation of the base polymer. The experimental results clearly showed through different techniques (FTIR and DS) that the most effective additive against the radiolytic oxidative ageing is Irganox 1076, thanks to its scavenging properties of radicals. On the contrary, the Irganox PS802 showed to be effective only when it is used in combination with the primary antioxidant (the synergistic effect).

Principal component analyses performed on both ATR-FTIR and DS results showed to be useful for derivation of some characteristics of the tested polymers. In particular, it is shown that PCA scores follow the evolution of material properties reaching particularly high values in the case of severely aged materials. In addition, the PCA scores resulted to be a function of the different additives and fillers inside the considered material. This permits the distinction of data clusters as a function of the additive type and the ageing level.

Future work on this topic will include the systematic application of the principal component analyses to other datasets (crosslinking grade, oxidative induction time, nuclear magnetic resonance, conductivity, etc.), in order to evaluate cable degradation for broader investigations.

ACKNOWLEDGEMENTS

The project leading to this application has received funding from the Euratom research and training programme 2014–2018 under grant agreement No. 755183. This publication reflects only the authors' view and the European Commission is not responsible for any use that may be made of the information it contains.

CONFLICT OF INTEREST

The authors declare no potential conflict of interests.

DATA AVAILABILITY STATEMENT

The data that support the findings of this study are available from the corresponding author upon reasonable request.

ORCID

Simone Vincenzo Suraci  <https://orcid.org/0000-0001-6258-5284>

Davide Fabiani  <https://orcid.org/0000-0003-4843-5508>

REFERENCES

1. The Paris Agreement. https://ec.europa.eu/clima/eu-action/international-action-climate-change/climate-negotiations/paris-agreement_it (Accessed Apr. 28, 2022)
2. Intergovernmental Panel on Climate Change. Climate Change 2014 Mitigation of Climate Change: Working Group III Contribution to the Fifth Assessment Report of the Intergovernmental Panel on Climate Change. Cambridge University Press, Cambridge (2014)
3. Glass, S.W., et al.: State of the Art Assessment of NDE Techniques for Aging Cable Management in Nuclear Power Plants FY201. United States (2015). <https://doi.org/10.2172/1242348>
4. Bowler, N., Liu, S.: Aging mechanisms and monitoring of cable polymers. *Int. J. Prognostics Health Manag.* 6(3), 2287 (2015)
5. Ferry, M., et al.: 3.16 - polymers in the nuclear power industry. In: KoningsStoller, R.J.M.R.E. (ed.) *Comprehensive Nuclear Materials*, 2nd ed, pp. 545–580. Elsevier, Oxford (2020)
6. Ferry, M., Miserque, F.: Radio-oxidation of electric cabled models: ageing evaluation at the atomic scale. *Energies* 15(5), 1631 (2022)
7. Assink, R.A., Gillen, K.T., Bernstein, R.: Nuclear Energy Plant Optimization (NEPO) Final Report on Aging and Condition Monitoring of Low-Voltage Cable Materials (2005). SAND2005-7331. 875986. <https://doi.org/10.2172/875986>
8. Liu, S., Fifield, L.S., Bowler, N.: Aging mechanisms of filled cross-linked polyethylene (XLPE) cable insulation material exposed to simultaneous thermal and gamma radiation. *Radiat. Phys. Chem.* 185, 109486 (2021)
9. Suraci, S.V., Li, C., Fabiani, D.: Dielectric spectroscopy as a condition monitoring technique for low-voltage cables: onsite aging assessment and sensitivity analyses. *Energies* 15(4), 1509 (2022)
10. Fabiani, D., Suraci, S.V.: Broadband dielectric spectroscopy: a viable technique for aging assessment of low-voltage cable insulation used in nuclear power plants. *Polymers* 13(4), 494 (2021)
11. Plaček, V., et al.: Dose rate effects in radiation degradation of polymer-based cable materials. *Nucl. Instrum. Methods Phys. Res. Sect. B Beam Interact. Mater. Atoms* 208, 448–453 (2003)
12. Fabiani, D., et al.: Innovative development and application of a stress-strength model for reliability estimation of aged LV cables for nuclear power plants. *IEEE Trans. Dielectr. Electr. Insul.* 28(6), 2083–2090 (2021)
13. Suraci, S.V., et al.: Multi scale aging assessment of low-voltage cables subjected to radio-chemical aging: towards an electrical diagnostic technique. *Polym. Test.* 103, 107352 (2021)
14. Suraci, S.V., et al.: Ageing assessment of XLPE LV cables for nuclear applications through physico-chemical and electrical measurements. *IEEE Access* 8, 27086–27096 (2020)
15. Linde, E., et al.: Dielectric spectroscopy as a condition monitoring technique for cable insulation based on crosslinked polyethylene. *Polym. Test.* 44, 135–142 (2015)
16. Mustafa, E., Afia, R.S.A., Tamus, Z.Á.: Condition monitoring uncertainties and thermal - radiation multistress accelerated aging tests for nuclear power plant cables: a review. *Period. Polytech. Elec. Eng. Comp. Sci.* 64(1), 20–32 (2019)
17. Mustafa, E., et al.: Implementation of non-destructive electrical condition monitoring techniques on low-voltage nuclear cables: I. Irradiation aging of EPR/CSPE cables. *Energies* 14(16), 5139 (2021)
18. Hettal, S., et al.: A new analytical model for predicting the radio-thermal oxidation kinetics and the lifetime of electric cable insulation in nuclear power plants. application to silane cross-linked polyethylene. *Polym. Degrad. Stabil.* 185, 109492 (2021)
19. Zhou, H., et al.: Aging behavior of flame-retardant cross-linked polyolefin under thermal and radiation stresses. *IEEE Trans. Dielectr. Electr. Insul.* 28(1), 303–309 (2021)
20. Gagliani, R., et al.: Capacitance Measurements for Nondestructive Testing of Aged Nuclear Power Plant Cable. In 46th Annual Review of Progress in Quantitative Nondestructive Evaluation (QNDE 2019), Portland, OR, USA, 14–19 July, 2019
21. Liu, S., Fifield, L.S., Bowler, N.: Towards aging mechanisms of cross-linked polyethylene (XLPE) cable insulation materials in nuclear power plants. In: 2016 IEEE Conference on Electrical Insulation and Dielectric Phenomena (CEIDP), pp. 935–938 (2016)
22. Miyazaki, Y., Hirai, N., Ohki, Y.: Effects of heat and gamma-rays on mechanical and dielectric properties of cross-linked polyethylene. *IEEE Trans. Dielectr. Electr. Insul.* 27(6), 1998–2006 (2020)
23. Liu, S., et al.: Quantitative analysis of changes in antioxidant in cross-linked polyethylene (XLPE) cable insulation material exposed to heat and gamma radiation. *Polym. Degrad. Stabil.* 156, 252–258 (2018)
24. Ohki, Y., Ishii, H., Hirai, N.: Degradation of soft epoxy resin for cable penetrations induced by simulated severe accidents. *Energies* 14(21), 6932 (2021)
25. Kemari, Y., et al.: Correlations between structural changes and dielectric behavior of thermally aged XLPE. *IEEE Trans. Dielectr. Electr. Insul.* 26(6), 1859–1866 (2019)
26. Hedir, A., et al.: Thermal ageing effects on polypropylene properties. In: 2019 IEEE Conference on Electrical Insulation and Dielectric Phenomena (CEIDP), pp. 130–133 (2019)
27. Colombani, J., et al.: A FTIR/chemometrics approach to characterize the gamma radiation effects on iodine/epoxy-paint interactions in Nuclear Power Plants. *Anal. Chim. Acta* 960, 53–62 (2017)
28. Maléchaux, A., et al.: Influence of gamma irradiation on electric cables models: study of additive effects by mid-infrared spectroscopy. *Polymers* 13(9), 1451 (2021)
29. Suraci, S.V., Fabiani, D.: Aging modeling of low-voltage cables subjected to radio-chemical aging. *IEEE Access* 9, 83569–83578 (2021)
30. Kremer, F., Schönhals, A. (eds.) *Broadband Dielectric Spectroscopy*. Springer Berlin Heidelberg, Berlin (2003). <https://doi.org/10.1007/978-3-642-56120-7>
31. Wold, S., et al.: Multi-way principal components-and PLS-analysis. *J. Chemometr.* 1(1), 41–56 (1987)
32. Saunier, J., et al.: Polymorphism of Irganox 1076®: discovery of new forms and direct characterization of the polymorphs on a medical device by Raman microspectroscopy. *Eur. J. Pharm. Biopharm.* 75(3), 443–450 (2010)
33. Xu, A., Roland, S., Colin, X.: Physico-chemical characterization of the blooming of Irganox 1076® antioxidant onto the surface of a silane-crosslinked polyethylene. *Polym. Degrad. Stabil.* 171, 109046 (2020). <https://doi.org/10.1016/j.polymdegradstab.2019.109046>
34. Dorey, S., et al.: Identification of Chemical Species Created during γ -irradiation of Antioxidant Used in Polyethylene and Polyethylene-co-vinyl Acetate Multilayer Film. *J Appl Polym Sci.* 137(43), 49336 (2020)

35. Xu, A., Roland, S., Colin, X.: Physico-chemical analysis of a silane-grafted polyethylene stabilised with an excess of Irganox 1076®. Proposal of a microstructural model. *Polym. Degrad. Stabil.* 183, 109453 (2021)
36. Krimm, S.: Infrared Spectra of High Polymers. In: *Fortschritte Der Hochpolymeren-Forschung. Advances in Polymer Science*, vol 2/1, pp. 122. Springer, Berlin, Heidelberg (2006)
37. Favaro, L., et al.: Experimental and ab initio infrared study of χ - κ - and α -aluminas formed from gibbsite. *J. Solid State Chem.* 183(4), 901–908 (2010)
38. Frederickson, L.D.: Characterization of hydrated aluminas by infrared spectroscopy. *Anal. Chem.* 26(12), 1883–1885 (1954)
39. Socrates, G.: *Infrared and Raman Characteristic Group Frequencies: Tables and Charts*, 3rd ed. Wiley, Chichester (2001)
40. Adams, J.H.: Analysis of the nonvolatile oxidation products of polypropylene I. Thermal oxidation. *J. Polym. Sci. A-1 Polym. Chem.* 8(5), 1077–1090 (1970)
41. Gardette, M., et al.: Photo- and thermal-oxidation of polyethylene: comparison of mechanisms and influence of unsaturation content. *Polym. Degrad. Stabil.* 98(11), 2383–2390 (2013)
42. Suraci, S.V., Fabiani, D., Li, C.: Additive effect on dielectric spectra of crosslinked polyethylene (XLPE) used in nuclear power plants. In: 2019 IEEE Electrical Insulation Conference (EIC), pp. 410–413 (2019)
43. Suraci, S.V., Fabiani, D.: Aging assessment of insulating materials through broadband dielectric measurements: the appropriate frequency choice. In: 2021 IEEE Conference on Electrical Insulation and Dielectric Phenomena (CEIDP), pp. 32–35 (2021)
44. Hettal, S., et al.: Towards a kinetic modeling of the changes in the electrical properties of cable insulation during radio-thermal ageing in nuclear power plants. Application to silane-crosslinked polyethylene. *Polymers* 13(24), 4427 (2021)
45. Li, J., et al.: Investigation of hindered phenol antioxidant effects on the aging performance of cross-linked LDPE in the presence of copper. *Sci. Rep.* 10(1), 10189 (2020)
46. Allen, N.S., et al.: Ageing and stabilisation of filled polymers: an overview. *Polym. Degrad. Stab.* 61(2), 183–199 (1998)
47. Scott, G.: *Atmospheric Oxidation and Antioxidants*. Elsevier (1993). <https://doi.org/10.1016/C2009-0-15759-8>

How to cite this article: Suraci, S.V., et al.: Ageing evaluation of cable insulations subjected to radiation ageing: Application of principal component analyses to Fourier Transform Infra-Red and dielectric spectroscopy. *High Volt.* 1–14 (2022). <https://doi.org/10.1049/hve2.12239>